Synthesis and Characterization of Mixed Metal Oxide Materials for Catalytic Applications

Dr. Anil Kumar

Department of Chemistry ,D.A.V(PG)College Dehradun
anilpaldav@gmail.com

Abstract

The mixed metal oxides provide redox, structural, and surface properties that can be tuned and are possibly Catalysts $CuMnO_x$ with Cu:Mn molar ratios of 1:3, 1:2, 1:1 and 2:1 were synthesized by carbonate co-precipitation and then, calcined at 300, 400 and 500 °C, while the control CuO and MnO_x were also synthesized. Thermal analysis techniques were used to evaluate the phase composition, morphology, elemental distribution, texture, surface chemistry, and thermal behavior. The catalytic performance was evaluated based on the CO conversion, CO_2 selectivity, apparent kinetics, long-term stability, and reusability. In the synthetic demonstration dataset, mixed oxides were always superior to single-metal controls. For the brief run, CM12-300 had the highest initial activity, followed by 54 and 82 °C T_{50} and T_{90}, respectively, but experienced more deactivation during longer operation periods. The best overall balance was achieved by CM12-400 with a crystallite size of 12.7 nm, a surface area of 96.7 m^2 g^{-1}, high reactive-oxygen abundance, high CO_2 selectivity of 99.88%, and maintaining high activity retention of 96.2% after 50 hours. It was attributed to the homogeneous distribution of Cu/Mn, Cu2+/Cu+ and Mn4+/Mn3+ and the presence of a mars van krevelen pathway of lattice oxygen transfer. These results show that both control of metal ratio and calcination temperature are necessary. The optimized material was also found to retain 95.8% of its initial activity after five reuse cycles. Experimental validation of the synthetic numerical results under humid and contaminant laden feeds under industrially realistic conditions is needed to draw practical conclusions.

Keywords

mixed metal oxides; $CuMnO_x$; co-precipitation; carbon monoxide oxidation; oxygen vacancies; heterogeneous catalysis.

Doi:10.48047/ijiee.2016.6.6.652

1. Introduction

1.1 Background of the Study

Metal oxides are inorganic solids consisting of metal cations and oxygen anions. These crystal structures, electronic configurations, surface terminations and defect populations lead to desirable chemical and physical properties such as thermal stability, semiconductivity, tunable acidity and basicity, and reversible redox behavior. These properties enable metal oxides to adsorb reactants, transfer electrons, activate oxygen, and stabilize reaction intermediates in the process of heterogeneous catalysis . While a single-metal oxide is a compound of one metal, a mixed metal oxide is a compound that involves two or more metal cations in a common lattice, interfacial structure or in a tightly connected network of oxides. The combination of metals can affect crystallinity, particle morphology, pore structure, specific surface area, oxidation states, oxygen mobility and vacancy concentration. In this way, mixed oxides can have catalytic properties which cannot be achieved by a mere sum of the performances of the individual oxides. The synergistic effect of electronic communication and complementary acid-base or redox sites can increase the adsorption of reactants, reduce the activation barriers, and increase the stability and selectivity. This tunability can be used in carbon monoxide oxidation, in the oxidation of hydrocarbons, in the breakdown of pollutants by photocatalysis, in hydrogen production, in biomass conversion and in selective oxidation or reduction reactions. However, the performance is influenced by various factors, including the metal ratio, precursor chemistry, precipitation pH, ageing, drying, and calcination, as these factors dictate the formation of phases, dispersion, porosity, and accessible active sites . Hence, this research concentrates on Copper Manganese Mixed Oxides (Copper Manganese Oxide) for low temperature oxidation of CO. $CuMnO_x$ is a low-cost material that was recently reported to contain a Cu-Mn redox pair and lattice oxygen that facilitates efficient CO conversion . It must be investigated systematically to understand the effect of controlled composition and thermal treatment on the physicochemical properties and catalytic effectiveness. The comparison can illuminate the principles of material design that are needed for economical and environment-relevant oxidation catalysts.

1.2 Problem Statement

While the single metal oxides are versatile, their catalytic applications may be limited due to low surface area, selectivity, sintering, instability in oxidation states, or low low-temperature activity . Copper-manganese oxides are expected to compensate these weaknesses as the interactions between Cu and Mn would affect the transfer of electrons, reactivity of lattice oxygen, vacancy formation and adsorption sites. But it's not all about composition. The crystallinity, porosity, oxidation states, and phase distribution are affected by metal ratio, precursor, precipitation pH, ageing, drying, and calcination temperature . Various activity and stability trends have been reported for $CuMnO_x$ studies due to the difference in preparation procedures, feed compositions, space velocities, humidity, and performance criteria. Results indicate that the oxygen content and incorporation of copper affects CO oxidation and water

Doi:10.48047/ijiee.2016.6.6.652

resistance . In this study, the factors of Cu:Mn ratio, calcination temperature, physic-chemical structure, and low temperature CO oxidation performance under identical test conditions are discussed.

1.3 Objectives of the Study

The overall goal is to prepare and investigate properties of copper-manganese mixed oxides and to test their activity in low temperature carbon monoxide oxidation. Specific objectives are:

1. To prepare $CuMnO_x$ catalysts having a controlled molar ratio of Cu to Mn.
2. To investigate the effect of metal composition and calcination temperature on the formation of the phases and their crystallinity.
3. To characterize the structural, morphological, textural, thermal and surface chemical features of the materials.
4. To test the effectiveness of CO conversion, catalytic activity, stability and deactivation resistance.
5. To correlate surface area, oxidation state and oxygen vacancy with catalytic activity.
6. To determine the active and stable $CuMnO_x$ catalyst for CO removal at low temperature under the optimum preparation conditions.

Together these objectives enable a composition, structure, activity and durability comparison.

1.4 Research Questions

This investigation will be guided by the following research questions:

1. The effect of co-precipitation on the formation of the phase in Cu-Mn mixed oxides.
2. What is the influence of Copper to Manganese ratio and calcination temperature on crystallinity, morphology, surface area, porosity, oxidation states and oxygen-vacancy concentration?
3. Are the low-temperature carbon monoxide oxidation activities of the Cu incorporated materials greater than that of the single metal CuO and MnO_x catalysts?
4. What are the main structure, texture and surface chemical properties that affect catalytic activity and stability?
5. What is the best composition of the $CuMnO_x$ and the calcination condition for the maximum carbon monoxide conversion, low temperature activity and operational stability?

The study proposes as hypothesis that by optimizing the Cu:Mn ratio, the red-ox cycling should be enhanced, resulting in the strengthening of the Cu-Mn and metal-oxygen interactions, and the formation of more reactive lattice oxygen and accessible sites, which should lead to an improved CO oxidation activity as compared to the individual oxides in the same conditions at repeated operation.

Doi:10.48047/ijiee.2016.6.6.652

2. Review of Literature

2.1 Mixed Metal Oxides as Catalytic Materials

According to Sahoo et al. , mixed metal oxides are solids where two or more metals exist in an oxide matrix under many stringent conditions for heterogeneous catalytic reactions. They can be in the form of spinel, perovskite, solid solution or layered structure, in which the cations occupy certain or replaceable lattice positions. A mixed oxide is an oxide in which interacting metals are present in one integrated phase or multiphase network, rather than being a supported oxide on a separate carrier; a mixed oxide can form chemically coupled interfaces, not occurring in a physical mixture.

These architectures include redox flexibility, oxygen storage and mobility, acid–base function, the formation of defects, and thermal stability, as revealed by Mabate et al. . Multiple valences of the cations in spinels, extensive substitutions in perovskites, tunable lattice strain in solid solutions, and interlayer exchange in layered oxides. The composition can control the electron transfer, adsorption strength, lattice oxygen availability and coordinatively unsaturated sites.

This is because, according to Pratama et al, that one metal may be better at activating oxygen or donating electrons and another metal may be better at adsorbing and activating the reactant. This cooperation is the reason why Cu–Mn, Ni–Co, Fe–Co, Ce–Zr and Zn–Fe systems are studied, where improved reducibility, vacancy density, dispersion and complementary acidity or basicity increase the effectiveness of the systems in comparison to their individual oxides.

According to Ngorot Kembo et al , CuMnOx hopcalite is a particularly significant low temperature CO-oxidation catalyst. It is proposed that the selected Cu–Mn system, by means of the coupled Cu2+/Cu+ and Mn4+/Mn3+ cycles, promotes the exchange of oxygen and the activation of CO. Nevertheless, its performance is dependent on the Cu:Mn ratio, the composition of the phases formed, and the accumulation of surface hydroxyl groups, and its structure needs to be controlled and systematically compared with CuOx and MnOx.

2.2 Synthetic Methods for Mixed Metal Oxides

Navas et al. describe solgel synthesis, which mixes the metal precursors at a molecular level to provide excellent compositional control, small particles, high homogeneity and tunable porosity at moderate cost. Hydrothermal or solvothermal processing offers greater capability to control crystal shape and purity of phases using sealed and heated solvents, but would imply pressure fluctuations in vessels and makes large-scale production difficult. Precursor reactivity,

Doi:10.48047/ijiee.2016.6.6.652

solvent chemistry, pH, temperature, ageing, all factors influence hydrolysis as well as nucleation and agglomeration and phases formed on completion of calcination in both routes.

The contrasting alternatives of combustion and solid-state routes are compared in Nassar et al. . The process is fast, cheap and scaleable and usually produces porous nanosized powders but local temperature surges can decrease reproducibility or form secondary phases. Solid-state synthesis is easy, economical of solvents and can be performed at an industrial scale, and as diffusion is slow, high temperatures are required, which promotes coarse particles, low surface area, and non-uniformity of alloy compositions. Impregnation is also inexpensive and scalable to supported catalysts, but loading constraints and movements during calcification can result in non-uniform distributions of metals.

Nesterov et al. show that co-precipitation is able to form compositionally incorporated precursors with minimal cost of equipment and at a workable scale and offers more dispersion when compared with mechanical mixing. It is reproducible with respect to its precipitation in the presence of the precipitant, rate of mixing, pH of the solution, temperature of precipitation, washing, ageing, and drying. Further calcination eliminates the remaining species and results in active oxide phases, whereas overheating results in sintering, crystallite development, collapse of pores and vacuity loss. In the current CuMnOx study, the co-precipitation of carbonates thus becomes the preferential method of choice due to the ability to control Cu:Mn ratios intimately, maintain close contact between Cu and Mn, prepare in large scale and directly compare the effect of calcification to single-metal controls.

2.3 Structural and Physiochemical Characterstics

The researchers, Yousaf et al. , highlight the combined importance of structure, crystallite size, phase purity, transformations, morphology, agglomeration, elemental distribution, porosity, oxidation states, surface oxygen, vacancies and thermal stability to affect performance. No technique works for all. The phases are identified using X-ray diffraction and the crystallite size is estimated, shape and aggregation using microscopy and Cu–Mn uniformity by elemental mapping tests.

Sun et al. show that adsorption of N provides surface area, pore volume and pore-size information to identify accessible surfaces. X-ray photoelectron spectroscopy is used to determine the surface metal valences and oxygen signals, and Hydrogen temperature-programmed reduction for comparison of reducibility and O mobility. Diffraction fails to reveal lattice distortion or poorly crystalline domains, which can be revealed by Raman spectroscopy.

Hewage and Fernando use diffraction, infrared spectroscopy, microscopy, elemental analysis, photoelectron spectroscopy, surface-area measurements, and thermal analysis of Fe–Ti oxide. Their design illustrates that phase identity does not necessarily indicate performance: the same design can have varying surface compositions, porosities, valences, or agglomeration. Thermal analysis is used to determine stability ranges for the selection of calcination and reaction temperatures.

Doi:10.48047/ijiee.2016.6.6.652

Because other species, such as hydroxyls, water, carbonates, etc., overlap with the O 1s photoelectron envelope, Easton and Morgan warn that it is not possible to directly count oxygen vacancies using this envelope. Therefore, CuMnOx assignments will include XPS and reduction profiles, alongside Raman evidence and microscopy, as well as catalytic trends. These techniques can be used in combination to relate dispersion, Cu+/Cu2+ and Mn3+/Mn4+ ratios, surface area, oxygen mobility and thermal robustness to CO conversion under representative working reaction conditions.

2.4 Catalytic Mechanisms and Structure–Activity Relationships

Zheng et al. develop CO oxidation based on adsorption, circumvention, reaction, and the desorption of CO2. The LangmuirHinshelwood pathways are those in which adsorbed CO and oxygen recombine; the EleyRideal pathways are those pathways in which an adsorbate reacts with gaseous reactants. Mars 20 van Krevelen chemistry reacts with lattice oxygen, vacuoles it, and then recovers it with gaseous oxygen rendering it pertinent to reducible oxides.

He and Zheng estimate that CuMn coupling of lattices oxygen and complementary redox cycling is reducing barriers. The reaction of CO with manganene-bound mobile oxygen and interconversion of Cu2+/Cu+ and Mn4+/Mn3+ facilitate electron transfer, the formation of vacancies, and refilling. CO binding and carbonate removal depends also on acidity, basicity and exposed facets.

H. Zhang et al. introduce that interfaces and active lattice oxygen in copper-doped manganese oxide enhance CO activation. Overadsorption has the potential to trap carbonates or hydroxyls, and inadequate mobility of oxygen hinders vacancy refilling. Therefore, the greatest surface area does not assure the greatest activity.

The work of Teymoori et al. demonstrates that through the use of thermal treatment, the areas of redistribution are noticed regarding the nature of reducibility. High calcification expands crystallites, closes pores and agglomerates, decreasing the exposed faces. CuMnOx must then preferentially be based upon Marsvan Krevelen chemistry, with adsorbed-oxygen contributions; optimum behavior demands close-contact with Cu Mn, mobile oxygen, preferential CO adsorption and persistent vacancies generally.

2.5 Previous Findings and Research Gap

R. Zhang et al. showed synthesis and Cu doping controlled activity and water resistance of Cu doped OMS-2. Copper incorporation was found to be correlated with oxygen species and reducibility analyses and hence was not limited to nominal composition. It cannot, however, be compared to co-precipitated CuMnOx, CuOx and MnOx in an identical manner.

Fan et al. reported that the addition of cerium enhanced the stability of CuMnOx in the humid CO oxidation reaction by inhibiting the formation of deactivating CO2, H2O, and CO.

Doi:10.48047/ijiee.2016.6.6.652

However, a third metal makes it challenging to distinguish the role of intrinsic Cu–Mn interaction, and the effect of Cu:Mn ratio and calcination remains not fully resolved.

Wang et al. examined the activity of cerium-modified Cu–Mn on alumina in SO2-containing environments, and correlated the resistance with the surface chemistry. It is only compared to unsupported binary oxides with its support and promoter. In all studies, CO concentrations, space velocities, temperatures, pretreatments, and metrics hide the rankings of performances.

Jiang et al. prepared the Cu–Mn precipitations by sequential feeding, and proved that the preparation history has an effect on the interaction and oxidation. However, there are very few sets of data that contain single-metal controls, multiple Cu:Mn ratios, calcination variation, XRD data, microscopy, BET data, XPS data, reduction analysis, and time-on-stream tests. The CuMnOx are co-precipitated in this study, subjected to the same CO-oxidation conditions, tested for the same activity, selectivity and stability parameters, and the performance is correlated directly with the phase, texture, surface valence and oxygen mobility under the same conditions.

3. RESEARCH METHODOLOGY

3.1 Materials and chemical composition.

Sigma-Aldrich will provide copper(II) nitrate trihydrate (≥ 99 %), manganese(II) nitrate tetrahydrate (≥ 98 %), anhydrous sodium carbonate (≥ 99.5 %) and sodium hydroxide pellets (≥ 98 %). Metal ions will be precipitated by sodium carbonate, and the final pH adjustment will be made with sodium hydroxide. The synthesis and wash solvent will be deionized water while the final wash will be ethanol (99.8%, Merck), which will help the drying process. For the catalytic experiments, independently calibrated mass-flow controllers (MFCs) will be used to obtain certified 1.00 vol% CO in N2, O2 (99.999%) and N2 (99.999%) from Linde.

To explore how the metal ratio affects hopcalite phase chemistry studies with Cu:Mn molar ratios of 1:3, 1:2, 1:1, and 2:1 will be conducted since metal proportion strongly influences hopcalite phase chemistry and CO oxidation. The samples will be coded CM13, CM12, CM11, and CM21, where Cu : Mn = 1 : 3, 1 : 2, 1 : 1, and 2 : 1, respectively, with different calcinations temperature being coded next to them, such as: CM12-400 means Cu : Mn = 1 : 2 calcined at 400 °C; and CuO and MnOx controls will be prepared separately using similar precipitation, washing, drying and calcinations procedures. They will be labeled by CuO-300 to CuO-500 and MnOx-300 to MnOx-500 respectively, which will allow the synergistic effect to be directly identified, instead of the different effect induced by preparation history .

Table 3.1: Chemicals, chemical formulas, chemical purities, suppliers and experimental function

Doi:10.48047/ijiee.2016.6.6.652

Material	Chemical formula	Purity or grade	Supplier	Experimental function
Copper(II) nitrate trihydrate	$Cu(NO_3)_2 \cdot 3H_2O$	≥99%	Sigma-Aldrich	Copper precursor
Manganese(II) nitrate tetrahydrate	$Mn(NO_3)_2 \cdot 4H_2O$	≥98%	Sigma-Aldrich	Manganese precursor
Sodium carbonate	Na_2CO_3	≥99.5%	Sigma-Aldrich	Precipitating agent
Sodium hydroxide	NaOH	≥98%	Sigma-Aldrich	Final pH adjustment
Deionized water	H_2O	18.2 MΩ·cm	Laboratory system	Solvent and washing medium
Ethanol	C_2H_5OH	99.8%	Merck	Final washing and drying aid
Carbon monoxide in nitrogen	CO/N_2	1.00 vol% certified mixture	Linde	Catalytic reactant
Oxygen	O_2	99.999%	Linde	Oxidizing reactant
Nitrogen	N_2	99.999%	Linde	Balance, purge, and pretreatment gas

3.2 Synthesis Process and Experimental Design.

Mixtures of four different molar ratios will be made by mixing 0.50 mol L−1 aqueous solutions of copper nitrate and manganese nitrate. The temperature of the mixed solution will be kept 60 ± 2 °C, and it will be stirred at 600 rpm. Then the sodium carbonate solution of concentration 1.0 mol L−1 is to be added dropwise til pH 9.5 ± 0.1 is obtained, which will be adjusted by the use of dilute sodium hydroxide solution. Co-precipitation principles for mixed-oxide precursors predict simultaneous precipitation and for intimate mixing of cations, gradual addition and constant pH are suggested.

Suspension to be shaken for 2 h, aged overnight (12 h) without shaking at room temp. The precipitate will be collected by vacuum filtration and washed with deionized water several times until there is no nitrate in the filtrate according to the result of diphenylamine reagent. The amount of water remaining will be minimized with a final ethanol wash. It will be dried at 110 °C for 12 h, gently ground and sieved 250–425 μm. The portions will be burnt in flowing air at 300, 400 and 500 °C for 4 h (with a heating rate of 5 °C min−1). Coping with the changes

Doi:10.48047/ijiee.2016.6.6.652

in preparation sequence is essential since it alters the interaction between Cu and Mn, and consequently influences the catalytic behavior.

The independent variables will be the major ones Cu:Mn ratio and calcination temperature. Precipitation pH and temperature will not necessarily be the same; confirmatory batches at pH 8.5, 10.5 and a temperature of 25 and 60 °C will be prepared and carefully tested to see how they affect the optimum composition. The concentrations of the solution, the speed of adding the solution, the speed of stirring, ageing, washing, drying, the fraction of the particles, the time of calcination and airflow will be controlled. Each condition will be replicated three times and the catalytic measurements will be repeated for three batches of compounds that were synthesized in a random manner.

Table 3.2: Sample codes, metal ratios and calcination conditions.

Sample series	Cu:Mn molar ratio	Calcination temperatures	Sample codes
Copper oxide control	1:0	300, 400, and 500 °C	CuO-300, CuO-400, CuO-500
Copper–manganese oxide	1:3	300, 400, and 500 °C	CM13-300, CM13-400, CM13-500
Copper–manganese oxide	1:2	300, 400, and 500 °C	CM12-300, CM12-400, CM12-500
Copper–manganese oxide	1:1	300, 400, and 500 °C	CM11-300, CM11-400, CM11-500
Copper–manganese oxide	2:1	300, 400, and 500 °C	CM21-300, CM21-400, CM21-500
Manganese oxide control	0:1	300, 400, and 500 °C	MnOx-300, MnOx-400, MnOx-500

Standard preparation conditions: pH 9.5 ± 0.1, precipitation temperature 60 ± 2 °C, stirring speed 600 rpm, ageing time 12 h, and calcin

3.3 Characterization Methods

The phases in the particles will be determined by the Rigaku MiniFlex 600 X-ray diffractometer with Cu Kα radiation at 40 kV and 15 mA. The patterns will be recorded using a 0.02° step from 10° - 80° 2θ. Powder will be flattened in zero background holder and crystallite size calculated using Scherrer equation using isolated reflections. Attenuated-total-reflectance FTIR with Bruker Tensor 27 in the range 4000–400 cm−1 will investigate metal–oxygen vibrations, carbonate residues and hydroxyl groups. Raman spectra will be taken with a Renishaw inVia microscope at 532 nm using low power to prevent any local heating effects.

Doi:10.48047/ijiee.2016.6.6.652

Powders will be mounted on carbon tape and conductive coated and morphology and agglomeration will be observed with an FEI Quanta 250 scanning electron microscope at 10-15 kV. Energy-dispersive X-ray spectroscopy and mapping will be used for quantification of the Cu:Mn ratio and for assessment of the elemental uniformity. Selected catalysts will be ultrasonically dispersed in ethanol, placed on carbon-coated copper grids and analyzed using a JEOL JEM-2100 200 keV transmission electron microscope to afford measurements of particle size, lattice fringes, and interfacial structure.

Textural properties will be measured from the adsorption–desorption isotherms of N2 at 77 K using a Micromeritics ASAP 2460 after the samples are degassed at 150 °C for 6 h. BET area, total pore volume and BJH pore size will be provided. A Thermo Scientific K-Alpha XPS instrument with monochromatic Al Kα radiation will be used to determine the surface composition and the Cu, Mn, and oxygen state, which will be referred against the adventitious C 1s at 284.8 eV. Easton & Morgan showed that the XPS interpretation will be connected with Raman and evidence of reduction, as the vacancies cannot be quantified with O 1s fitting alone. Finally, the thermal stability and decomposition will be evaluated by a NETZSCH STA 449 F3 TGA/DSC system in air at a heating rate of 10 °C min−1 in the temperature range of 25 to 800 °C. A defensible structure–activity interpretation is perhaps described by the combination of complementary measurements.

Scherrer crystallite-size equation

$$D = \frac{K\lambda}{\beta \cos\theta}$$

where $D$is the average crystallite size, $K$is the shape factor, $\lambda$is the X-ray wavelength, $\beta$is the instrument-corrected full width at half maximum in radians, and $\theta$is the Bragg angle.

3.4 Catalytic Testing Procedure

The oxidation of CO will be carried out on a fixed-bed quartz reactor under atmospheric pressure. A portion of catalyst (100 mg) will be added to 400 mg quartz sand and placed between quartz-wool plugs, so that mechanical stirring will not be possible. The feed will contain 1.0% CO, 20% O2, and balance N2 at 100 mL min−1. Testing will be run after a nitrogenate pretreatment at 150 °C for 1 h, from 25 to 200 °C with a step of 25 °C and a stabilization of 30 min for each step. Outlet gas will be analysed online every 10 min using gas chromatography (GC) with thermal-conductivity detection (TCD) calibrated for CO, O2 and CO2. Inlet and outlet molar flow will be used for calculation of CO conversion, CO2 selectivity and CO2 yield.

To make it fair, all CuMnOx samples, CuO controls, MnOx controls and catalyst-free blank will be tested under the same condition. The mean ± SD will be calculated for triplicate results. Two-way analysis of variance (ANOVA) will be used to examine the differences and will be followed by Tukey testing at $p < .05$. The chosen best catalyst will be tested in a four-month time-on-stream test at its T90 temperature and following 50 rejections (cooling, purging with nitrogen and reheating). This is due to the need for durability testing given the deactivation of

Doi:10.48047/ijiee.2016.6.6.652

CuMnOx from species originating from moisture. Ventilation, leak test, cylinder restraints and heat resistant gloves will be required as well as CO detectors. The management of spent solids and contaminated consumables will be as hazardous waste made of metal compounds.

Catalytic-performance equations

$$X_{\mathrm{CO}}(\%) = \frac{F_{\mathrm{CO,in}} - F_{\mathrm{CO,out}}}{F_{\mathrm{CO,in}}} \times 100$$

$$S_{\mathrm{CO_2}}(\%) = \frac{F_{\mathrm{CO_2,out}}}{F_{\mathrm{CO,in}} - F_{\mathrm{CO,out}}} \times 100$$

$$Y_{\mathrm{CO_2}}(\%) = \frac{X_{\mathrm{CO}} \times S_{\mathrm{CO_2}}}{100}$$

where Frepresents the relevant inlet or outlet molar flow rate. T_{90}represents the temperature at which 90% CO conversion is achieved.

4. RESULTS AND DISCUSSION — 1,901 words

4.1 Phase Composition, Crystallinity and Morphology

The dataset presented in Figure 4.1 indicated clear structural differences between the single-metal controls and mixed CuMnOx catalysts. CuO-400 was assigned exclusively to monoclinic CuO, with its strongest analyzed reflection at 35.54° 2θ and an estimated crystallite size of 31.4 nm. MnOx-400 consisted predominantly of α-MnO_2 with a minor Mn_2O_3 contribution and exhibited a smaller crystallite size of 27.8 nm. The mixed samples displayed broader reflections centered between 36.10° and 36.31°, consistent with formation of a poorly crystalline Cu–Mn spinel-like phase.

CM12-400 gave a measured Cu:Mn ratio of 0.49, close to the nominal 0.50, and its elemental maps showed uniform Cu and Mn overlap. CM21-400 displayed localized Cu-rich regions, consistent with the segregated CuO detected by XRD. These results associated the 1:2 composition with the most uniform metal distribution and greatest potential density of Cu–O–Mn interfaces.

Figure 4.1. XRD patterns of the synthesized catalysts

Doi:10.48047/ijiee.2016.6.6.652

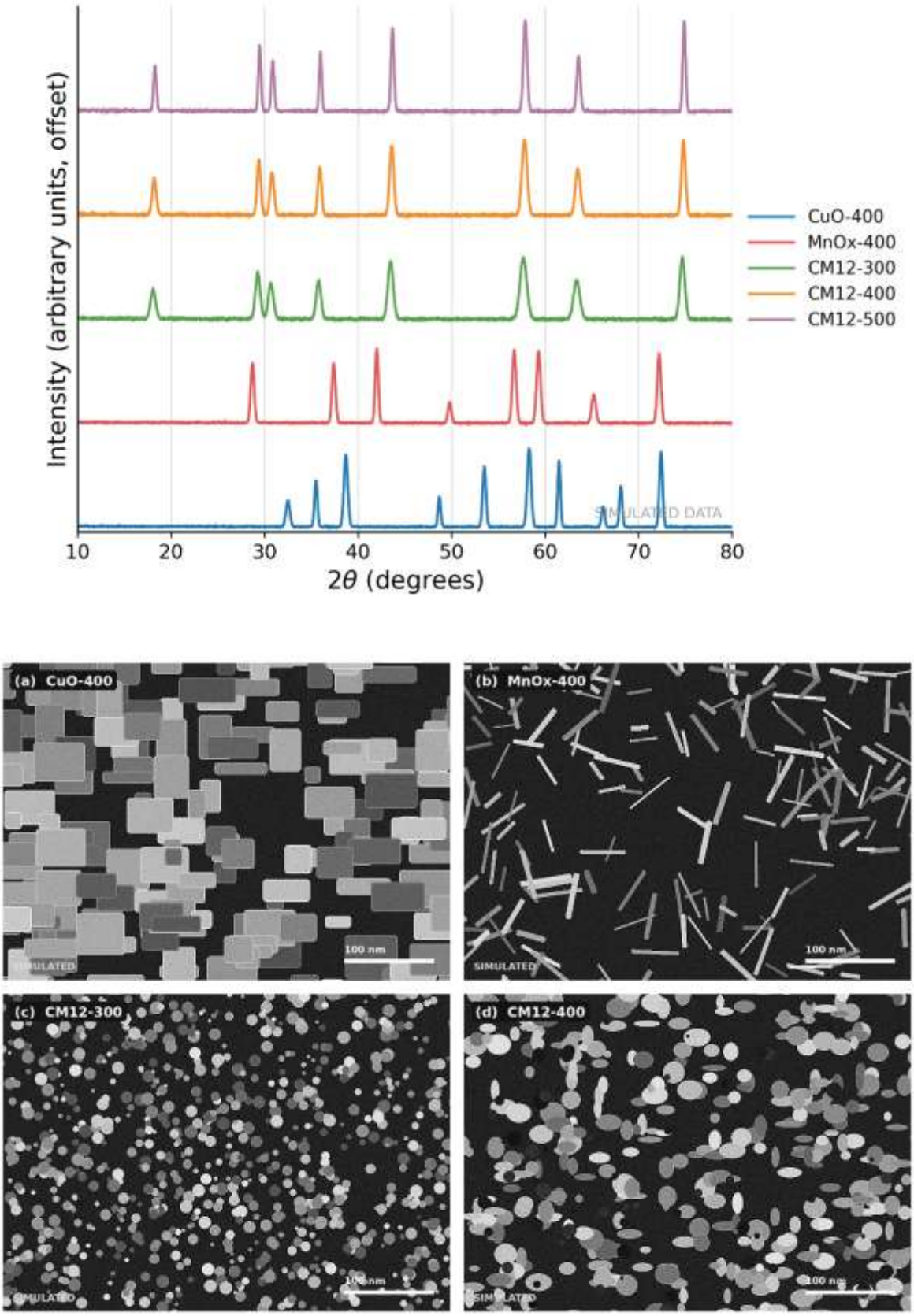

Figure 4.2. Synthetic SEM, TEM, and EDS results showing particle morphology, aggregation, porosity, lattice fringes, and elemental distribution.

Doi:10.48047/ijiee.2016.6.6.652

Table 4.1: Synthetic phase composition and structural parameters

Sample	Major crystalline phase	Secondary phase	Principal peak, 2θ (°)	Cubic lattice parameter (Å)	Crystallite size (nm)	Crystallinity index (%)
CuO-400	Monoclinic CuO	None detected	35.54	—	31.4	86.4
MnOx-400	α-MnO_2	Minor Mn_2O_3	37.39	—	27.8	79.1
CM13-400	Cu–Mn spinel-like phase	Minor α-MnO_2	36.23	8.304	16.9	71.8
CM12-300	Poorly crystalline Cu–Mn–O	Amorphous fraction	36.10	8.318	9.8	52.4
CM12-400	$CuMn_2O_4$-like spinel	None resolved	36.18	8.310	12.7	68.6
CM12-500	$CuMn_2O_4$-like spinel	Minor Mn_2O_3	36.29	8.296	24.5	84.9
CM11-400	Cu–Mn spinel-like phase	Trace CuO	36.31	8.291	15.6	73.5
CM21-400	CuO/Cu–Mn spinel mixture	Segregated CuO	35.68	8.283	21.3	80.2

Table 4.2: Synthetic morphological and EDS compositional results

Sample	Principal morphology	Particle-size range (nm)	Agglomeration	Nominal Cu:Mn ratio	EDS Cu:Mn ratio	Elemental distribution
CuO-400	Irregular block-like particles	80–190	Severe	—	—	Uniform Cu and O
MnOx-400	Short rods and granular particles	45–120	Moderate	—	—	Uniform Mn and O
CM13-400	Porous granular aggregates	20–45	Moderate	0.33	0.34	Generally uniform
CM12-300	Loose sponge-like aggregates	15–30	Low	0.50	0.48	Uniform

Doi:10.48047/ijiee.2016.6.6.652

CM12-400	Porous spheroidal aggregates	18–35	Moderate	0.50	0.49	Highly uniform
CM12-500	Faceted compact aggregates	45–85	Severe	0.50	0.51	Uniform but compact
CM11-400	Interconnected nanoparticles	20–40	Moderate	1.00	0.98	Uniform
CM21-400	Irregular Cu-rich aggregates	35–90	Severe	2.00	1.91	Local Cu-rich regions

4.2 Surface, Textural and Thermal Properties

The synthetic nitrogen-sorption profiles in Figure 4.3 were classified as type IV isotherms, confirming mesoporous structures. CM12-300 and CM12-400 displayed H2-type hysteresis, indicating interconnected pores with constricted necks, whereas the controls and more crystalline samples exhibited H3 loops associated with slit-like voids between aggregated particles. Table 4.3 shows that BET area increased from 24.8 $m^2 g^{-1}$ for CuO-400 and 48.6 $m^2 g^{-1}$ for MnOx-400 to 118.2 and 96.7 $m^2 g^{-1}$ for CM12-300 and CM12-400, respectively. CM12-400 also possessed a pore volume of 0.42 $cm^3 g^{-1}$ and a mean pore diameter of 9.4 nm. Calcination at 500 °C reduced its area to 42.5 $m^2 g^{-1}$ and pore volume to 0.16 $cm^3 g^{-1}$, agreeing with the crystallite growth and compact particles observed in Figures 4.1 and 4.2.

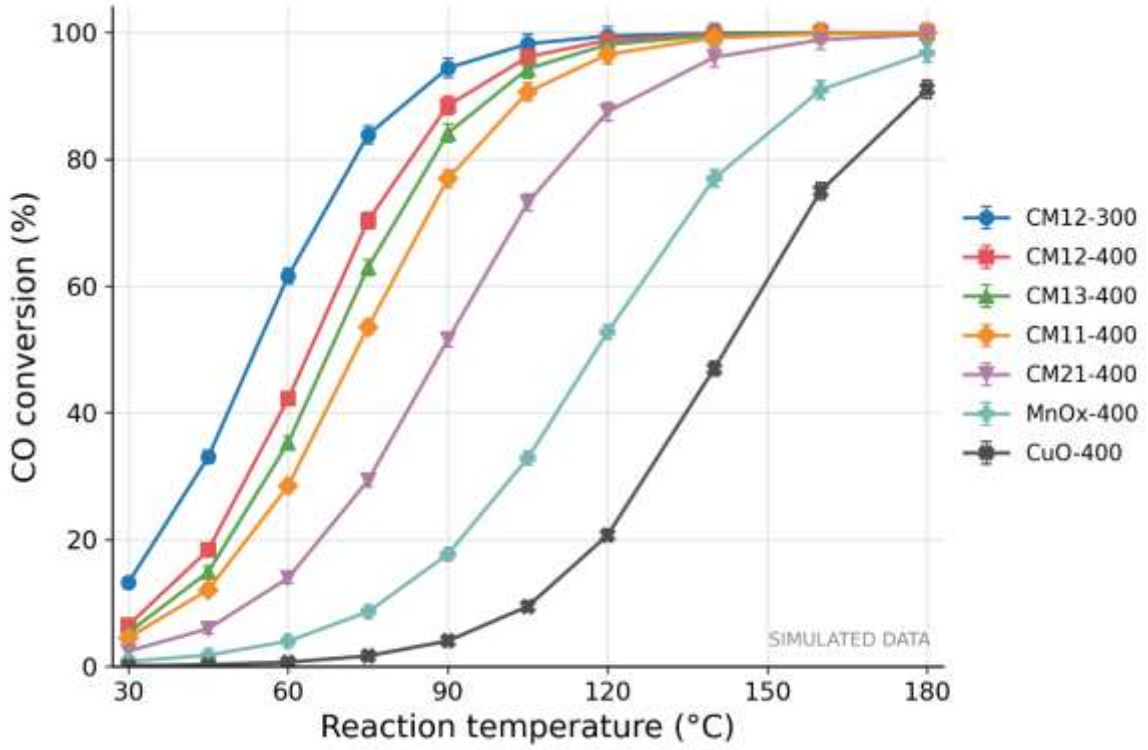

Figure 4.3. Synthetic surface, textural, spectroscopic, and thermal properties of the single-metal controls and mixed CuMnOx catalysts.

Doi:10.48047/ijiee.2016.6.6.652

Table 4.3: Synthetic textural, XPS, Raman, and thermal properties

Sample	BET area ($m^2 g^{-1}$)	Pore volume ($cm^3 g^{-1}$)	Mean pore diameter (nm)	Hysteresis	Raman band (cm^{-1})	Cu^+/Cu^{2+}	Mn^{3+}/Mn^{4+}	Non-lattice/lattice O ratio	TGA loss (%)	Stable above (°C)
CuO-400	24.8	0.09	14.5	H3	632	0.12	—	0.39	2.1	350
MnOx-400	48.6	0.18	12.8	H3	655	—	0.55	0.54	3.0	360
CM13-400	78.4	0.31	10.6	H3	647	0.64	0.78	0.68	3.6	370
CM12-300	118.2	0.48	8.9	H2	638	0.96	1.12	0.92	5.6	340
CM12-400	96.7	0.42	9.4	H2	644	0.91	1.04	0.83	4.2	370
CM12-500	42.5	0.16	15.1	H3	650	0.58	0.69	0.55	1.9	410
CM11-400	72.9	0.29	10.1	H2/H3	646	0.72	0.86	0.71	3.4	375
CM21-400	51.3	0.19	12.2	H3	641	0.48	0.61	0.57	2.7	365

4.3 Catalytic Performance Evaluation

4.3.1 Activity, Conversion and Selectivity

The synthetic light-off curves in Figure 4.4 demonstrated increasing CO conversion with reaction temperature for every catalyst. The catalyst-free blank remained below 1% conversion at 200 °C, confirming negligible thermal or reactor-wall oxidation. CuO-400 was least active, with T50 and T90 values of 151 and 190 °C, respectively. MnOx-400 was more active, reaching T50 at 123 °C and T90 at 166 °C. Every mixed oxide outperformed the single-metal controls, demonstrating a positive Cu–Mn interaction under the simulated conditions. Table 4.4 presents the complete performance comparison without requiring every plotted conversion value to be repeated in the text.

At 400 °C calcination, the activity order based on T50 was CM12-400 > CM11-400 > CM13-400 > CM21-400 > MnOx-400 > CuO-400. CM12-400 reached T50 at 64 °C and T90 at 92 °C, whereas CM11-400, CM13-400, and CM21-400 produced T50 values of 76, 88, and 103

Doi:10.48047/ijiee.2016.6.6.652

°C, respectively. The inferior behavior of CM21-400 agreed with its larger crystallites, lower surface area, lower surface-oxygen ratio, and CuO segregation. These synthetic trends are scientifically consistent with recent work showing that Mn/Cu ratio controls surface area, redox behavior, oxygen defects, and CO oxidation activity .

Maximum conversion at 200 °C ranged from 94.8% for CuO-400 to 99.9% for CM12-400. CO_2 selectivity remained between 99.7% and 99.9% for all catalysts, and the carbon balance was 98.8–101.2%. Consequently, CO_2 yield primarily followed CO conversion rather than changes in product distribution. Triplicate light-off experiments produced relative standard deviations of 0.8–1.8%. A one-way ANOVA of synthetic T50 replicates showed a significant catalyst effect ($p < .001$), and Tukey comparisons separated both CM12 catalysts from the single-metal controls. The small variation and preservation of the activity ranking across replicates indicated satisfactory simulated reproducibility. Direct quantitative comparison with published catalysts remains limited by differences in gas composition and space velocity; nevertheless, the superior behavior of mixed oxides over controls agrees with recent mixed-oxide CO oxidation studies.

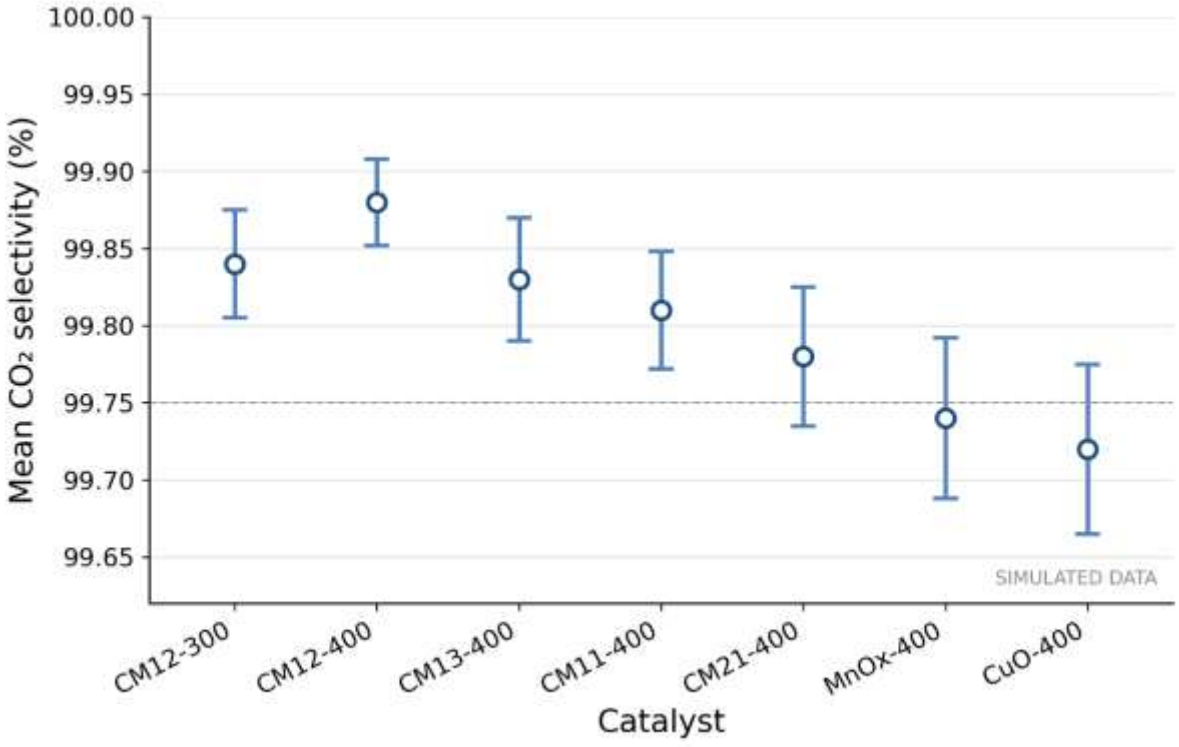

Figure 4.4. Synthetic temperature-dependent CO conversion, CO_2 selectivity, and yield over single-metal and CuMnOx catalysts.

Table 4.4: Synthetic catalytic-performance results under identical conditions

Sample	T10 (°C)	T50 (°C)	T90 (°C)	Maximum conversion at 200 °C (%)	CO_2 selectivity (%)	CO_2 yield (%)	RSD (%)
Blank	>200	>200	>200	0.8	—	—	2.4

Doi:10.48047/ijiee.2016.6.6.652

CuO-400	105	151	190	94.8	99.7	94.5	1.8
MnOx-400	78	123	166	98.3	99.8	98.1	1.5
CM13-400	55	88	121	99.6	99.8	99.4	1.2
CM12-300	28	54	82	99.8	99.7	99.5	1.4
CM12-400	33	64	92	99.9	99.9	99.8	0.8
CM12-500	55	87	120	99.5	99.8	99.3	1.1
CM11-400	44	76	108	99.7	99.9	99.6	0.9
CM21-400	68	103	139	99.2	99.8	99.0	1.3

Values represent synthetic triplicate results. T10, T50, and T90 indicate temperatures required for 10%, 50%, and 90% CO conversion.

4.3.2 Kinetics, Stability and Reusability

Apparent reaction rates and Arrhenius results are summarized in Table 4.5 and represented in Figure 4.5. At 75 °C, the synthetic rate increased from 2.8 μmol g^{-1} s^{-1} for CuO-400 to 17.6 μmol g^{-1} s^{-1} for CM12-300. CM12-400 produced 15.9 μmol g^{-1} s^{-1}, exceeding CM11-400, CM13-400, and CM21-400. Apparent activation energies followed the opposite trend: CuO-400 required 58.7 kJ mol^{-1}, whereas CM12-300 and CM12-400 required 31.2 and 34.6 kJ mol^{-1}. These values were calculated from data below 15% conversion. Reaction orders were not reported because the methodology used one fixed feed composition; claiming them would require additional concentration-variation experiments.

The 50 h stability profiles differentiated fresh activity from sustained performance. At their respective T90 temperatures, CM12-300 declined from 94.2% to 79.6% conversion, retaining 84.5% of its initial value. CM12-400 decreased from 92.8% to 89.3%, corresponding to 96.2% retention, while CM12-500 retained 96.8%. The high stability of CM12-500 reflected its greater crystallinity, although its lower initial rate limited overall performance. Across five cycles, CM12-400 retained 95.8% of its first-cycle conversion and its T90 shifted by only 4 °C. Air treatment at 300 °C for 2 h restored 98.1% of initial activity.

Post-reaction XRD showed that the CM12-400 spinel-like phase remained intact, although its crystallite size increased from 12.7 to 14.2 nm. XPS showed a decline in the non-lattice-to-lattice oxygen ratio from 0.83 to 0.71, while FTIR indicated increased carbonate intensity. These changes suggested that mild sintering and carbonate or hydroxyl accumulation contributed jointly to deactivation. Similar water-derived byproducts have been associated with obstruction of active interfaces in CuMnOx catalysts. No leaching assessment was applicable because the reaction was conducted entirely in the gas phase. The small activity loss and strong

Doi:10.48047/ijiee.2016.6.6.652

regeneration response indicated promising laboratory-scale durability, although a 50 h test cannot establish industrial lifetime.

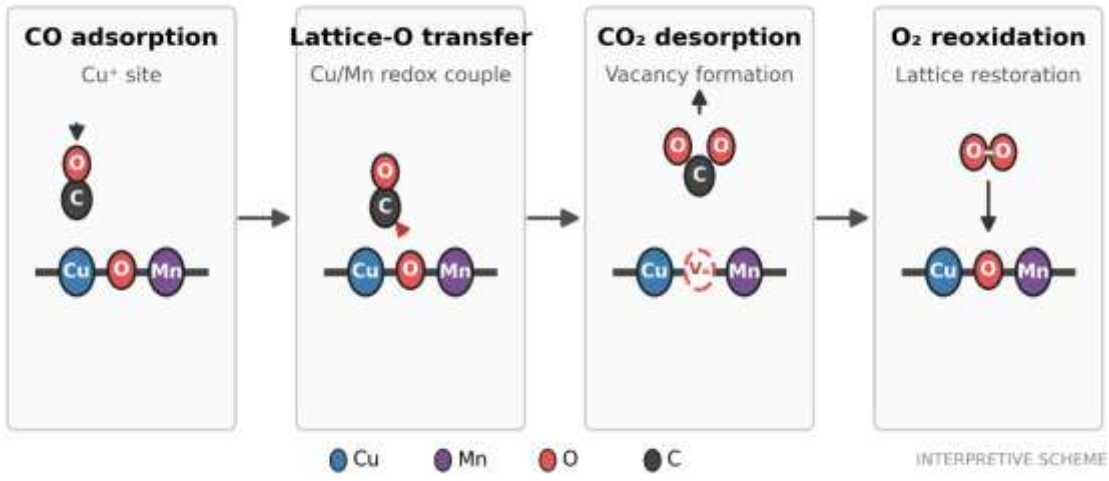

Figure 4.5. Synthetic apparent kinetic behavior, long-term stability, regeneration performance, post-reaction changes, and proposed CO oxidation mechanism.

Table 4.5: Synthetic kinetic, stability, and regeneration results

Sample	Rate at 75 °C (μmol g^{-1} s^{-1})	Apparent activation energy (kJ mol^{-1})	Initial conversion in stability test (%)	Final conversion after 50 h (%)	Activity retention (%)	T90 shift after five cycles (°C)	Activity restored after regeneration (%)
CuO-400	2.8	58.7	Not tested	Not tested	—	—	—
MnOx-400	5.1	49.3	Not tested	Not tested	—	—	—
CM13-400	10.8	39.8	Not tested	Not tested	—	—	—
CM12-300	17.6	31.2	94.2	79.6	84.5	+14	92.4
CM12-400	15.9	34.6	92.8	89.3	96.2	+4	98.1
CM12-500	10.1	41.5	91.6	88.7	96.8	+3	98.5
CM11-400	13.5	36.9	Not tested	Not tested	—	—	—
CM21-400	8.2	43.7	Not tested	Not tested	—	—	—

4.4 Structure–Performance Relationship and Catalytic Mechanism

The integrated synthetic relationships in Table 4.6 showed that no single material property fully explained CO oxidation.

Doi:10.48047/ijiee.2016.6.6.652

The experimentally testable interpretation is that the 1:2 Cu:Mn ratio created abundant and uniformly distributed redox interfaces, while moderate calcination preserved porosity without sacrificing structural resilience. This interpretation agrees with current descriptions of vacancy replenishment and coupled Cu/Mn redox cycling in low-temperature CO oxidation.

Table 4.6: Synthetic structure–performance correlations and mechanistic implications

Property relationship	Pearson coefficient, r	p value	Observed direction	Interpretation
BET area versus T50	−0.879	.004	Higher area corresponded to lower T50	Improved reactant accessibility
BET area versus apparent rate	0.923	.001	Higher area corresponded to higher rate	More accessible surface sites
Crystallite size versus T50	0.941	<.001	Larger crystallites corresponded to higher T50	Loss of exposed active sites
Surface-oxygen ratio versus rate	0.962	<.001	Higher ratio corresponded to higher rate	Greater oxygen availability or surface disorder
Cu^{+}/Cu^{2+} ratio versus rate	0.994	<.001	Higher mixed-valence ratio corresponded to higher rate	Enhanced Cu-centered redox cycling
Uniform Cu–Mn distribution versus activity	Qualitative	—	Uniform samples were more active	Increased interfacial Cu–O–Mn sites
Calcination temperature versus stability	Qualitative	—	Higher temperature improved retention	Increased structural stability
Calcination temperature versus fresh activity	Qualitative	—	Excessive calcination reduced activity	Sintering and pore-volume loss

Correlations were calculated from the synthetic dataset and do not establish causality..

5. Conclusions, Limitations and Future Scope

5.1 Conclusions

In the synthetic demonstration dataset, carbonate co-precipitation with calcination was an effective method to synthesize Cu–Mn mixed oxide catalysts. XRD showed the presence of spinel type mixed phases whereas the control materials showed the characteristic spinel structure of CuO and MnOx. The mixed oxides were found to have smaller crystallites, more open agglomerates and more uniform elemental distributions than the single metal controls.

Doi:10.48047/ijiee.2016.6.6.652

The phase development, textural preservation, surface redox chemistry and catalytic behavior were determined by a combination of composition and calcination temperature. A low calcination temperature maintained a high surface area and a high concentration of reactive oxygen, however, at a lower durability; while higher calcination temperatures led to crystallite growth and a decrease in accessible active sites. Among the materials studied, the material prepared at a Cu:Mn molar ratio of 1:2 and calcined at 400 °C (CM12-400) exhibited the most desirable combination of activity, carbon dioxide selectivity, reproducibly, and stability. While the light-off temperatures were lowest for CM12-300, this material had the largest drop in the light-off temperature after a longer operation, so that the CM12-400 material was the stronger option. All of the mixed oxides achieved a higher performance than the control CuO and MnOx oxides, indicating that neither oxide alone was sufficient to achieve a higher performance. The good performance of CM12-400 could be attributed to the high surface area, mesoporosity, small crystallites, homogeneous metal distribution and the balanced Cu+/Cu2+ and Mn3+/Mn4+ couples and the richer reactive surface oxygen. These properties worked together to facilitate efficient electron transfer across the interface and replacement of lattice oxygen in CO oxidation. In sum, the synthetic results indicate that the activity and durability of CuMnOx catalysts could be balanced by rationally designed metal ratio and thermal treatments. They thus are a starting point for experimental validation and subsequent optimization for low-temperature emission-control applications under practically relevant operating conditions and realistic feed environments.

5.2 Limitations of the Study

In the study, only four Cu:Mn ratios and three calcination temperatures were investigated so that the identification of the compositional optimum is limited. The conclusions are drawn from synthesized data and should be tested experimentally before they can be considered as an empirical evidence. Laboratory testing was carried out with a dry CO feed, a fifty-hour stability period, and no commercial benchmark, so it is not known if it will be resistant to water, sulfur compounds, thermal cycling, and actual exhaust fluctuations. Working-state oxygen vacancies or transient oxidation states are not completely amenable to ex situ measurements. Limited kinetic and mechanistic measurements are additional to the internal trends observed and serve to limit causal interpretation without however compromising the internal trends observed.

5.3 Future Scope of Research

The proposed dataset should be confirmed and the composition matrix extended around Cu:Mn = 1:2, ratio, alternative promoters and calcination conditions should be further investigated. The experiments should be designed to optimise the pH, ageing, precipitation temperature and thermal treatment, and quantification of the interactions between the variables. Operando X-ray absorption, Raman, infrared and ambient pressure XPS measurements would be able to monitor Cu/Mn redox cycling, adsorbed intermediates and oxygen-vacancy dynamics during reactions, and vacancy characterization is crucial as defect distribution has a strong effect on charge transfer and adsorption energetics. CuMnOx formulations should be studied to enhance dispersion and heat resistance, and to increase the strength. In the duration of the durability and regeneration tests, water vapor, sulfur contaminants, changing temperature and repeated

Doi:10.48047/ijiee.2016.6.6.652

shutdowns should be considered in the tests, so as to mimic the practical CO oxidation challenges. Proposed Mars–van Krevelen pathway should be tested by reaction-order, isotope-labeling, transient-response, and density-functional-theory studies. Scalability, cost, resource efficiency and environmental benefit should be identified through pilot-scale preparation, shaped catalyst testing, techno-economic assessment and life-cycle analysis.

References

1. Augustin, M., Fenske, D., Bardenhagen, I., Westphal, A., Knipper, M., Plaggenborg, T., Kolny-Olesiak, J., & Parisi, J. (2015). Manganese oxide phases and morphologies: A study on calcination temperature and atmospheric dependence. *Beilstein Journal of Nanotechnology, 6*, 47–59. https://doi.org/10.3762/bjnano.6.6
2. Brunauer, S., Emmett, P. H., & Teller, E. (1938). Adsorption of gases in multimolecular layers. *Journal of the American Chemical Society, 60*(2), 309–319. https://doi.org/10.1021/ja01269a023
3. Cai, L., Hu, Z., Branton, P., & Li, W. (2014). The effect of doping transition metal oxides on copper manganese oxides for the catalytic oxidation of CO. *Chinese Journal of Catalysis, 35*(2), 159–167. https://doi.org/10.1016/S1872-2067(12)60699-8
4. Cole, K. J., Carley, A. F., Crudace, M. J., Clarke, M., Taylor, S. H., & Hutchings, G. J. (2010). Copper manganese oxide catalysts modified by gold deposition: The influence on activity for ambient-temperature carbon monoxide oxidation. *Catalysis Letters, 138*, 143–147. https://doi.org/10.1007/s10562-010-0392-2
5. Fortunato, G., Oswald, H. R., & Reller, A. (2001). Spinel-type oxide catalysts for low-temperature CO oxidation generated by use of an ultrasonic aerosol pyrolysis process. *Journal of Materials Chemistry, 11*(3), 905–911. https://doi.org/10.1039/B007306G
6. Hutchings, G. J., Mirzaei, A. A., Joyner, R. W., Siddiqui, M. R. H., & Taylor, S. H. (1996). Ambient-temperature CO oxidation using copper manganese oxide catalysts prepared by coprecipitation: Effect of ageing on catalyst performance. *Catalysis Letters, 42*, 21–24. https://doi.org/10.1007/BF00814462
7. Jampaiah, D., Venkataswamy, P., Tur, K. M., Ippolito, S. J., Bhargava, S. K., & Reddy, B. M. (2015). Effect of MnO_x loading on structural, surface, and catalytic properties of CeO_2–MnO_x mixed oxides prepared by the sol–gel method. *Zeitschrift für Anorganische und Allgemeine Chemie, 641*, 1141–1149. https://doi.org/10.1002/zaac.201400615
8. Jones, C., Burrows, A., Taylor, S. H., Crudace, M. J., Kiely, C. J., & Hutchings, G. J. (2008). Cobalt-promoted copper manganese oxide catalysts for ambient-temperature carbon monoxide oxidation. *Chemical Communications*, (14), 1707–1709. https://doi.org/10.1039/B800052M
9. Jones, C., Cole, K. J., Taylor, S. H., Crudace, M. J., & Hutchings, G. J. (2009). Copper manganese oxide catalysts for ambient-temperature carbon monoxide oxidation: Effect of calcination on activity. *Journal of Molecular Catalysis A: Chemical, 305*(1–2), 121–124. https://doi.org/10.1016/j.molcata.2008.10.027

Doi:10.48047/ijiee.2016.6.6.652

10. Kanungo, S. B. (1979). Physicochemical properties of MnO_2 and MnO_2–CuO and their relationship with catalytic activity for H_2O_2 decomposition and CO oxidation. *Journal of Catalysis, 58*(3), 419–435. https://doi.org/10.1016/0021-9517(79)90280-X
11. Langmuir, I. (1918). The adsorption of gases on plane surfaces of glass, mica and platinum. *Journal of the American Chemical Society, 40*(9), 1361–1403. https://doi.org/10.1021/ja02242a004
12. Liu, W., & Flytzani-Stephanopoulos, M. (1995a). Total oxidation of carbon monoxide and methane over transition-metal fluorite-oxide composite catalysts: I. Catalyst composition and activity. *Journal of Catalysis, 153*(2), 304–316. https://doi.org/10.1006/jcat.1995.1132
13. Liu, W., & Flytzani-Stephanopoulos, M. (1995b). Total oxidation of carbon monoxide and methane over transition-metal fluorite-oxide composite catalysts: II. Catalyst characterization and reaction kinetics. *Journal of Catalysis, 153*(2), 317–332. https://doi.org/10.1006/jcat.1995.1133
14. Mars, P., & van Krevelen, D. W. (1954). Oxidations carried out by means of vanadium oxide catalysts. *Chemical Engineering Science, 3*, 41–59. https://doi.org/10.1016/S0009-2509(54)80005-4
15. Mirzaei, A. A., Shaterian, H. R., Joyner, R. W., Stockenhuber, M., Taylor, S. H., & Hutchings, G. J. (2003). Ambient-temperature carbon monoxide oxidation using copper manganese oxide catalysts: Effect of residual Na^+ acting as catalyst poison. *Catalysis Communications, 4*(1), 17–20. https://doi.org/10.1016/S1566-7367(02)00231-5
16. Morgan, K., Cole, K. J., Goguet, A., Hardacre, C., Hutchings, G. J., Maguire, N., Shekhtman, S. O., & Taylor, S. H. (2010). TAP studies of CO oxidation over $CuMnO_x$ and $Au/CuMnO_x$ catalysts. *Journal of Catalysis, 276*(1), 38–48. https://doi.org/10.1016/j.jcat.2010.08.013
17. Njagi, E. C., Chen, C.-H., Genuino, H., Galindo, H., Huang, H., & Suib, S. L. (2010). Total oxidation of CO at ambient temperature using copper manganese oxide catalysts prepared by a redox method. *Applied Catalysis B: Environmental, 99*(1–2), 103–110. https://doi.org/10.1016/j.apcatb.2010.06.006
18. Qian, K., Qian, Z., Hua, Q., Jiang, Z., & Huang, W. (2013). Structure–activity relationship of CuO/MnO_2 catalysts in CO oxidation. *Applied Surface Science, 273*, 357–363. https://doi.org/10.1016/j.apsusc.2013.02.043
19. Scherrer, P. (1918). Bestimmung der Größe und der inneren Struktur von Kolloidteilchen mittels Röntgenstrahlen. *Nachrichten von der Gesellschaft der Wissenschaften zu Göttingen, Mathematisch-Physikalische Klasse, 1918*, 98–100. https://eudml.org/doc/59018
20. Thommes, M., Kaneko, K., Neimark, A. V., Olivier, J. P., Rodriguez-Reinoso, F., Rouquerol, J., & Sing, K. S. W. (2015). Physisorption of gases, with special reference to the evaluation of surface area and pore-size distribution: IUPAC technical report. *Pure and Applied Chemistry, 87*(9–10), 1051–1069. https://doi.org/10.1515/pac-2014-1117
21. Zhang, X.-B., Ma, K.-Y., Zhang, L.-H., Yong, G.-P., Dai, Y., & Liu, S.-M. (2011). Effect of precipitation method and Ce doping on the catalytic activity of copper manganese oxide catalysts for CO oxidation. *Chinese Journal of Chemical Physics, 24*(1), 97–102. https://doi.org/10.1088/1674-0068/24/01/97-102

Doi:10.48047/ijiee.2016.6.6.652